

Published in final edited form as:

Ultrasound Med Biol. 2011 February ; 37(2): 189–197. doi:10.1016/j.ultrasmedbio.2010.11.001.

AXIAL-SHEAR STRAIN ELASTOGRAPHY FOR BREAST LESION CLASSIFICATION: FURTHER RESULTS FROM *IN VIVO* DATA

Arun K. Thittai¹, Jose-Miguel Yamal², Louise M Mobbs³, Christina M Kraemer-Chant³,
Srinivasa Chekuri¹, Brian S Garra³, and Jonathan Ophir¹

¹ Department of Diagnostic and Interventional Imaging, the University of Texas Medical School, Houston, Texas, USA

² Division of Biostatistics, The University of Texas School of Public Health, Houston, Texas, USA

³ Department of Radiology, Fletcher Allen Health Care, Burlington, VT, USA

Abstract

The purpose of this work was to investigate the potential of the normalized axial-shear strain area (NASSA) feature, derived from axial-shear strain elastograms (ASSE), for breast lesion classification of fibroadenoma and cancer. This study consisted of previously-acquired *in vivo* digital RF-data of breast lesions. A total of 33 biopsy-proven malignant tumors and 30 fibroadenoma cases were included in the study that involved 3 observers blinded to the original BIRADS®-ultrasound scores. The observers outlined the lesions on the sonograms. The ASSEs were segmented and color-overlaid on the sonograms, and the NASSA feature from the ASSE was computed semi-automatically. Receiver operating characteristic (ROC) curves were then generated and the area under the curve (AUC) was calculated for each observer performance. A logistic regression classifier was built to compare the improvement in the AUC when using BIRADS scores plus NASSA values as opposed to BIRADS scores alone. BIRADS score ROC had an AUC of 0.89 (95% CI = 0.81 – 0.97). In comparison, the average of the AUC for all the three observers using ASSE feature alone was 0.84. However, the AUC increased to 0.94 (average of 3 observers) when BIRADS score and ASSE feature were combined. The results demonstrate that the NASSA feature derived from ASSE has the potential to improve BIRADS breast lesion classification of fibroadenoma and malignant tumors.

Keywords

Breast lesions; Axial strain; Axial-shear strain; Benign; Cancer; Classification; Elastography; Fibroadenoma; Ultrasound

INTRODUCTION

Ultrasound (US) elastography was introduced by Ophir et al. (1991) as a technique to image the stiffness variation in soft-tissues. The technique involves acquiring US (RF/envelope)

Contact: Arun K. Thittai, PHD, The University of Texas Medical School, Department of Diagnostic and Interventional Imaging, Ultrasonics Laboratory, 6431 Fannin St., Houston, TX 77030, USA, 713.500.7651 Direct, 713.500.7694 Fax, Arun.K.Thittai@uth.tmc.edu.

Publisher's Disclaimer: This is a PDF file of an unedited manuscript that has been accepted for publication. As a service to our customers we are providing this early version of the manuscript. The manuscript will undergo copyediting, typesetting, and review of the resulting proof before it is published in its final citable form. Please note that during the production process errors may be discovered which could affect the content, and all legal disclaimers that apply to the journal pertain.

signals from an imaging plane before and after a small quasi-static compression. Typically, the pre- and post- compression frames are processed to generate images of local strain, commonly known as *elastograms*. When the elastogram depicts axial strain values, it is referred to as an *axial strain elastogram* (Ophir et al. 1999).

Based on the axial strain elastograms alone, elastography has been shown to be useful in a wide variety of clinical applications including breast lesion classification (Céspedes et al. 1993, Hiltawsky et al. 2001). The utility of elastography for the reduction of the rate of unnecessary breast biopsies has been demonstrated by several groups (Garra et al. 1997, Regner et al. 2006, Barr 2006, Itoh et al. 2006, Cho et al. 2008). Most of these reports have utilized the size discrepancy between sonographic and elastographic lesion appearance, along with/without strain contrast measures (Garra et al. 1997, Regner et al. 2006, Barr 2006, Burnside et al. 2007). Some of them have used a scoring system based on strain distribution patterns (Itoh et al. 2006, Cho et al. 2008).

However, these measures from axial strain elastograms exploit only the size discrepancy between the sonographic and elastographic images of the tumor, which exists only in malignant cases. Nevertheless, it is also well-documented in the literature that benign fibroadenomas are typically mobile (implying loosely- bonded to the host tissue) compared to malignant tumors, which tend to be well adhered (firmly bonded) to the host tissue (cf. Fry 1954, Ueno et al. 1988, Bamber et al. 1988). Therefore, it is reasonable to hypothesize that additional information regarding the bonding conditions near lesion boundaries has the potential to improve the performance of the current standard of practice in breast lesion classification by ultrasound.

Axial strain is one of the 9 strain tensors that describe deformation in 3D. We have shown that in addition to axial strain it may be feasible to image another strain tensor in the form of axial-shear strain (ThitaiKumar et al. 2007). Note that the total shear strain, as defined in equation 1, is the sum of the axial-shear (first-term) and lateral-shear strain component.

$$\varepsilon_{x,y} = \left(\frac{\partial v}{\partial x} + \frac{\partial u}{\partial y} \right) \quad (1)$$

Where (u , v) are the lateral and axial displacement components along the x - (lateral direction) and y - (axial direction) axes, respectively.

The ultrasonic estimation of the lateral-shear strain is noisy compared to the estimation of the axial-shear component (ThitaiKumar et al. 2005). This fundamental limitation due to suboptimal sampling between ultrasound array beams also impacts traditional elastography and sonography. However, we have shown that imaging the axial-shear component alone results in quality images of an independent constitutive tissue parameter that relates directly to shear strain. The image depicting the axial-shear strain was referred to as axial-shear strain elastogram (ASSE). We demonstrated recently that the axial-shear strain distribution pattern around an inclusion is directly influenced by the bonding at the inclusion-background boundary using simulations, gelatin-phantom experiments, and breast lesions *in vivo* (ThitaiKumar et al. 2007). The *normalized axial-shear strain area* (NASSA) near the inclusion-background boundary is a feature that could be used to identify the boundary bonding conditions (ThitaiKumar et al. 2007, 2008). Results from the initial feasibility study that evaluated the potential of this feature to differentiate between benign and malignant tumors in the breast are encouraging (ThitaiKumar et al. 2008). However, the initial

feasibility study was restricted to a small number of *in vivo* cases (n=21) that precluded a detailed statistical analysis.

In this paper, we report on a larger follow up study done to investigate the potential of the NASSA feature to classify breast lesions into fibroadenoma and cancer, and therefore reduce unnecessary benign breast biopsies. We include the results of a statistical analysis performed to assess the improvement in the BIRADS-based breast lesion classification due to the addition of NASSA.

MATERIALS AND METHODS

In vivo data

We used *in vivo* digital RF-data of breast lesions that were acquired at University of Vermont by Dr. Garra's group. The patient study was HIPAA compliant and had appropriate IRB approvals. Informed consent was obtained from all participating patients who were informed that the RF-data collected would be used at a later time for the creation of *elastograms*. The sonograms used in this study were reconstructed from the selected RF frames. Patients who had a BIRADS score of 4 and above and were scheduled for a biopsy participated in elastographic data acquisition. In addition, patients with BIRADS score 3 who elected to get a biopsy were also included. The elastographic data were acquired using a Philips HDI-1000 ultrasound scanner operating at 5 MHz center frequency. The setup consisted of a precision digital motor system for controlled compressions. The acquisition protocol involved multi-compression with step sizes of 0.25%, up to a maximum total compression of 5% (Varghese et al. 1998). For each *in vivo* case, six acquisitions (three each in two orthogonal planes) were acquired. Thus, we had the option to use scan data from more than one scan plane per case. Note that we only reprocessed the archived data and no new data acquisition was done in the present study.

We had a total of 134 pathologically-confirmed cases in our database comprising of 35 malignant and 99 benign cases. Among the benign cases, we had several "normal fibrocystic changes" and other benign conditions such as complex cysts and 33 fibroadenomas. For this (blinded) observer study only patients with biopsy proven fibroadenoma or cancer were included. This was because previously reported simulation and phantom studies (ThitaiKumar et al. 2007) utilized boundary conditions that modeled fibroadenomas and cancers. In addition, we noticed from simulations (not published) that the axial-shear strain feature reported in the literature (ThitaiKumar et al. 2007) is technically valid only if the lesion is located at a depth that is at least 1 lesion diameter below the surface of compression, due to inadequate surrounding tissue availability near the proximal lesion boundaries. By removing those cases where the lesion was located close (less than one diameter) to surface of compression, we were left with 30 of the 35 malignant cases and with all 33 fibroadenoma cases for this study.

ASSE generation, display and feature of interest

The pre-compression and temporally stretched post-compression RF signals were processed to obtain ASSEs using algorithms detailed elsewhere (Céspedes et al. 1993, ThitaiKumar et al. 2008). For each case, ASSEs were obtained for all six scan planes; only one scan plane was chosen for the observer study (as described in Appendix A). The area of the axial-shear strain region, normalized by the area of the lesion in the corresponding sonogram was used as the *feature* of interest (i.e., NASSA- Normalized axial-shear strain area). Additional details from prior work that describe this feature are given in Appendix A. However, the method to determine the area of axial-shear strain region differed slightly from the previous study (ThitaiKumar et al. 2008). In the present study, the ASSE was displayed as a color-

overlay on the corresponding sonogram, which was used as an anatomical reference. The segmentation of the axial-shear strain region was done automatically based on the sonographic lesion outlined by the expert observer(s) (details in Appendix A).

Observer training and Image evaluation protocol

We engaged three volunteer observers. Observers 1 and 3 were registered diagnostic medical sonographers with at least 10 years experience in breast ultrasound, while observer 2 was a trained breast radiologist. Observer 2 had never been exposed to ASSEs while observers 1 & 3 had some familiarity. During training, the observers were presented with sample images of color ASSEs overlaid on the corresponding sonograms that are typical of fibroadenoma and of cancers. Example images from the training set are shown in figure 1. We used 5 cases each of fibroadenomas and cancers for observer training purposes. This included 2 example cancer data that were excluded. The observers participated in the study one week after the training date, and the testing set included the training cases. However, we removed the training cases from the testing cases during statistical analysis.

The sequence of steps taken in the observer study is illustrated in the flowchart in figure 2. A custom interactive software program written in MATLAB[®] (Mathworks, MA) was used. The software randomly selected a case from the dataset and displayed the corresponding sonogram. The observers either manually outlined the sonographic lesion or responded 'no', to indicate lack of adequate sonographic lesion visualization. The ASSE was segmented automatically (details in Appendix A) based on presence or absence of sonographic lesion outline and displayed as a color-overlay on the corresponding sonogram. The observers were given the option of modifying their initial sonographic lesion outline upon viewing the color overlaid ASSE. Next, the observers evaluated the ASSE for a characteristic axial-shear strain pattern and feature extraction. The axial-shear strain area near the lesion of interest was segmented automatically, but to improve its reliability the observers were allowed to manually outline it, using a computer mouse. For this reason, the feature extraction from ASSEs may be considered as a semi-automatic process. In figure 1 the automated segmentation as well as the observer's outline circumscribing this area can be seen. Note that the observers were instructed to pay attention to the axial-shear strain areas only near the proximal lesion boundary. This was because in some *in vivo* sonograms the echo signals distal to the tumor have a poor signal-to-noise ratio due to attenuation and shadowing effects. Consequently, we are not able to produce reliable images of axial-shear strains in these distal regions with current algorithms. Further, of the two proximal regions (red and blue) only the maximum area was used, instead of possibly averaging the two areas, to compute the NASSA feature value. Note that a larger axial-shear strain area is expected near firmly-bonded lesions (cancers); by using the maximum we gave preference to possible false positives rather than to false negatives (missing a cancer). Finally, the software proceeded to the next randomly selected case. The BIRADS scores were assigned after review of both the mammograms and the ultrasound imaging. All five breast imagers who participated in the study have a minimum of 15 years experience reading mammograms and ultrasound (range 15–32 years experience) and are MQSA certified mammogram readers. Note that the BIRADS score used were the ones assigned prior to the elastographic data acquisition and used here only in the statistical analysis while the observers were blinded to it.

Statistical analysis

Receiver Operator Characteristic (ROC) analysis was used to summarize the diagnostic performances of NASSA and BIRADS to predict the pathological classification. Because correlation from multiple observers reading the same images can result in a biased ROC curve for combined data, we instead took the average of the readers' specificity at fixed sensitivity values to combine the observer-specific ROC curves (Obuchowski 2007). The

BIRADS scores were coded as 3, 4, 4.25 (for 4a), 4.5 (for 4b), 4.75 (for 4c), and 5. The statistical packages 'R', version 2.6.2 (R Foundation for Statistical Computing, Vienna, Austria), and Stata (StataCorp LP, Stata Statistical Software: Release 10.1, College Station, TX: 2008) were used for the analysis.

RESULTS

Table 1 summarizes the response from each observer who participated in the study. It can be seen that the number of sonograms on which the observers was able to outline the lesion (blinded to the ASSE) was on an average only 72% of the 63 cases (2nd column, i.e., average of 44/63, 54/63, and 38/63). This percentage improved by an average 6.3% after looking at the ASSE (3rd column), demonstrating the utility of ASSE in confirming the lesion boundary and thereby improving sonographic lesion visualization. The observers later reported that looking at the sonogram from only one scan plane restricted their visualization of the lesion in a number of cases. The last column gives the number of cases for which the observers were able to identify a sonographic lesion and characteristic ASSE features. The average yield on the diagnostically useful cases from all the observers was 60.3%. This is further discussed in the next section.

Figure 3 shows the ROC curves based on each observer's ASSE feature value, compared to the ROC curve for the BIRADS score. BIRADS had an area under the curve (AUC) of 0.89 (95% CI = 0.81 – 0.97). In comparison, observer 1 had an AUC of 0.85 (95% CI = 0.72 – 0.98), observer 2 had an AUC of 0.87 (CI = 0.76, 0.98), and observer 3 had an AUC of 0.81 (CI = 0.66 – 0.96). In addition, the plot also shows the average ROC curve for the ASSE feature value over the three observers.

To explore ways to combine the BIRADS score and the ASSE feature value, we first examined the scatter plots of NASSA versus BIRADS. Figure 4 shows the scatter plot obtained for the three observers. We note that there is a significant separation of the two classes in the bivariate distribution for the observations with a BIRADS score of 4. For example, note that several fibroadenoma with a BIRADS score of 4 can be identified by small NASSA value and several malignant tumors with small NASSA value have a BIRADS score of 5.

We then applied a logistic regression method to combine the NASSA values and the BIRADS score into one classifier score (Cox 1958). A logistic regression model was fitted with the outcome being the pathology report and predictors being the NASSA feature and BIRADS score, for each observer. The posterior probability of having a positive pathology report was used as a new score for classification, incorporating both the NASSA and BIRADS information. The observer-specific ROC curves for NASSA + BIRADS are compared to BIRADS alone in Figure 5. We observed an increase in accuracy for the combined classifier (mean AUC = 0.94). Also shown in Figure 5 is the average ROC curve of the three logistic regression models using NASSA + BIRADS compared to BIRADS alone. The logistic regression coefficient estimates for the three observers are shown in Table 2.

Boxplots of the predicted values from a logistic regression model using NASSA value and the BIRADS scores as predictors are shown in figure 6. It can be seen that the differences between the classes are similar for the three observers and the scores were very well separated between the two classes. This suggests that the inter-observer variability may not be large.

We expected our results to be biased upwards (or over estimated) since we presented the results on the same data set that was used for training of the parameters in the model. To

obtain an estimate of how well the classifiers might perform on out-of-sample data, we performed leave-out-one cross-validation (Shao 1993). For each observer, we removed one observation at a time and trained the logistic regression model with the remaining observations. The model was used to predict the omitted observation's posterior probability of having a positive pathology report. The posterior probabilities for each observation were combined to give an out-of-sample estimate of the performance of the classifier. As expected, the mean AUC decreased from 0.96, but to our surprise ended up at 0.86, slightly lower than that of BIRADS alone (mean AUC = 0.88). We believe that the sample size might be too small to estimate the accuracy with great accuracy. The average ROC curve of the cross-validated scores is shown in Figure 7.

DISCUSSION

The results from the study demonstrate that the recently introduced ASSE may have a role in aiding the ultrasound classification of benign vs. malignant breast lesions. More importantly, the results based on adding the NASSA feature to the established BIRADS scores show an improvement in classification performance, as evident from increase in the AUC from 0.88 to 0.94. In recent years, several reports have shown that using regular axial elastograms alongside BIRADS improves the breast lesion classification performance (c.f. Burnside et al. 2007, Cho et al. 2008). Unlike axial elastograms that depicts information related to underlying tissue stiffness, ASSEs conveys information regarding lesion/host boundary bonding property (ThitaiKumar et al. 2007). Therefore, it is reasonable to expect that the additional ASSE feature could improve the BIRADS or BIRADS+ASE –based classification performance even further. So far we did not incorporate the axial elastograms into this study. The major focus of this work was to evaluate the ASSE feature and incorporating the axial elastogram presented some issues regarding the order of presenting the image and bias associated with doing so. Nevertheless, this is an important aspect that will be addressed in a larger study in the future.

Another important aspect to be noted is that for any new technique to improve patient care it needs to reliably place lesions such as fibroadenomas into BIRADS 2 so that biopsy can be avoided. Although our intention was not to test the separability of BIRADS 4 and 5 with this new feature, we reported the analysis that included all the cases that had pathology results available. In the future, when a larger number of biopsy-proven cases of fibroadenomas might be available, we can probably exclude the cases with BIRADS score 5. At this investigative stage though, it was of interest to see how the ASSE feature performed for the cases with BIRADS score 5 as well.

The summary of the observer responses given in Table 1 has at least two points of interest. First, it shows that the observers found that ASSE was helpful in depicting the sonographic lesion in approx. 13% (average) of the cases. This is consistent with the observation we reported earlier (ThitaiKumar et al. 2008). Second, notice that the observers outlined the lesion in the sonogram only on approximately 78% of the cases. The number of diagnostically useful cases reduced even further to only 60%, when the ASSE feature was not extractable. The poor yield can be attributed to the following limitations. Recall that the elastographic data were acquired for a previous study and were not optimized for ASSE. Furthermore, the data acquisition was done while the operator was blind to the axial elastograms and to the ASSE. This limitation was further compounded when the observers had only one scan plane for determining sonographic lesion, as opposed to the cine-loop of frames typically used in standard practice. Furthermore, the 5MHz center frequency transducer used is lower than what is typically used in breast imaging today. A higher frequency transducer would be expected to have yielded better quality images and therefore increased the number of diagnostically useful cases. Thus, the nature of data acquisition

restricted the number of cases that were eventually analyzed. It is noteworthy that despite these limitations, the ASSE features were still able to improve the AUC.

It is known that ultrasound imaging in general is operator dependent and suffers from inter-observer variability to a large extent (Rahbar et al. 1999, Sehgal et al. 2004). It is clear from figure 6 that there was an agreement in the operating points among the observers. This could be due to the semi-automated nature of the feature extraction as well as having only one scan plane to evaluate. Recall that the observers outlined the sonographic lesions; however, the ASSE is segmented automatically. Thus, inter-observer variability was minimized probably because of general agreement on the sonographic lesion appearance. However, we are aware that a larger future study should investigate inter-observer variability more closely.

We had 134 cases in our database that consisted of fibroadenomas, cancers and other benign conditions. In this study, we shortlisted only fibroadenomas and cancers that were good approximations to the model studied for ASSE (ThitaiKumar et al. 2008). Nevertheless, the potential of ASSE to identify other benign conditions with suitable adjustments to the model is desirable but was beyond scope of the current work. Since the study was limited only to fibroadenomas and cancers, there were insufficient data to do a formal training and testing of the logistic regression algorithms. Therefore, although these preliminary results are very promising, a formal study to train and test an algorithm should be conducted to evaluate the accuracy of the combined ASSE + BIRADS.

CONCLUSIONS

In summary, we have shown that features from recently-developed ASSE, which provides information regarding lesion/host bonding characteristics, may add to existing sonographic and elastographic feature sets that are used in routine clinical practice for tumor differentiation with ultrasound. ASSEs are complementary to and can be used alongside with other co-registered images like axial strain elastograms and sonograms, to better visualize and interpret tissue information in the region of interest. ASSEs can be generated simultaneously with axial elastograms and sonograms, thus inheriting their advantages of being non-invasive, inexpensive, and available in real-time and in perfect spatial registration. However, it must be understood that the present results are based on *in vivo* cases obtained earlier without ASSE feedback. Therefore, a larger study on data set acquired with ASSE feedback is in order to confirm the initial promise. In addition, recall that the data used in this study were acquired using a controlled-compression device and not freehand, as might be desired. This aspect will need to be addressed in the future.

Acknowledgments

The data used in this study were acquired previously for projects supported by NIH Program Projects grants P01-CA64597 and P01-EB02105. The current work was supported by NIH grant R21-CA135580. The authors would also like to thank the observers Elaine Khalil, MD, Karen Ophir, BS, RDMS, Charlene Waldron, RT, RDMS and Rhoda Reading, BS, RDMS, RVT, RT, who volunteered their time to participate in the study.

References

- Bamber JC, De Gonzalez L, Cosgrove DA, Simmons P, Davey J, McKinna JA. Quantitative evaluation of real-time ultrasound features of the breast. *Ultrasound Med Biol.* 1988; 14:81–87. [PubMed: 3055606]
- Barr, RG. Clinical applications of a real time elastography technique in breast imaging. *Proceedings of the Fifth International Conference on Ultrasonic Measurement and Imaging of Tissue Elasticity;* 2006. p. 112

- Burnside ES, Hall TJ, Sommer AM, Hesley GK, Sisney GA, Svensson WE, Fine JP, Jiang J, Hangiandreou NJ. Differentiating benign from malignant solid breast masses with US strain imaging. *Radiology*. 2007; 245 (2):401–410. [PubMed: 17940302]
- Céspedes I, Ophir J, Ponnekanti H, Maklad NF. Elastography: elasticity imaging using ultrasound with application to muscle and breast *in vivo*. *Ultrasonic Imaging*. 1993; 15 (2):73–88. [PubMed: 8346612]
- Cho N, Moon WK, Park JS, Cha JH, Jang M, Seong MH. Nonpalpable Breast Masses: Evaluation by US Elastography. *Korean J Radiol*. 2008; 9:111–118. [PubMed: 18385557]
- Cox DR. The regression analysis of binary sequences (with discussion). *Journal of the Royal Statistical Society, B*. 1958; 20:215–242.
- Fry KE. Benign lesions of the breast. *CA Cancer J Clin*. 1954; 4:160–161.
- Garra BS, Céspedes I, Ophir J, et al. Elastography of breast lesions: initial clinical results. *Radiology*. 1997; 202:79–86. [PubMed: 8988195]
- Hiltawsky KM, Kruger M, Starke C, Heuser L, Ermert H, Jensen A. Freehand ultrasound elastography of breast lesions: Clinical results. *Ultrasound Med Biol*. 2001; 27:1461–1469. [PubMed: 11750744]
- Itoh A, Ueno E, Tohno E, et al. Breast disease: clinical application of US elastography for diagnosis. *Radiology*. 2006; 239:341–350. [PubMed: 16484352]
- Obuchowski NA. New Methodological Tools for Multiple-Reader ROC Studies. *Radiology*. 2007; 243:10–12. [PubMed: 17392244]
- Ophir J, Céspedes I, Ponnekanti H, Yazdi Y, Li X. Elastography: a method for imaging the elasticity of biological tissues. *Ultrasonic Imaging*. 1991; 13(2):11–13.
- Ophir, J.; Céspedes, I.; Maklad, N.; Ponnekanti, H. Ultrasonic Tissue Characterization. In: Dunn, F., et al., editors. *Elastography: A Method for Imaging the Elastic Properties of Tissue in vivo*. Vol. Chapter 7. Springer Verlag; Tokyo: 1996. p. 118
- Ophir J, Alam SK, Garra BS, Kallel F, Konofagou EE, Krouskop TA, Varghese T. Elastography: Ultrasonic Estimation and Imaging of the Elastic Properties of Tissues. *Journal of Engineering in Medicine*. 1999; 213 (H3):203–233. [PubMed: 10420776]
- Rahbar G, Sie AC, Hansen GC, et al. Benign versus malignant solid breast masses: US differentiation. *Radiology*. 1999; 213:889–894. [PubMed: 10580971]
- Regner DM, Hesley GK, Hangiandreou NJ, et al. Breast lesions: evaluation with US strain imaging—clinical experience of multiple observer. *Radiology*. 2006; 238:425–437. [PubMed: 16436810]
- Sehgal MC, Cary WT, Kangas SA, Weinstein PS, Schultz MS, Arger HP, Conant FE. Computer-Based Margin Analysis of Breast Sonography for Differentiating Malignant and Benign Masses. *J Ultrason Med*. 2004; 23:1201–1209.
- Shao J. Linear model selection by cross-validation. *J Am Stat Assoc*. 1993; 88:486–494.
- ThittaiKumar A, Ophir J, Krouskop TA. Noise performance and signal-to-noise ratio of shear strain elastograms. *Ultrasonic Imaging*. 2005; 27:145–165. [PubMed: 16550705]
- ThittaiKumar A, Krouskop TA, Garra BS, Ophir J. Visualization of bonding at an inclusion boundary using axial shear strain elastography: A feasibility study. *Phys Med Biol*. 2007; 52:2615–2633. [PubMed: 17440256]
- Thittaikumar A, Mobbs LM, Kraemer-Chant CM, Garra BS, Ophir J. Breast Tumor Classification using axial shear strain elastography: a feasibility study. *Phys Med Biol*. 2008; 53:4809–4823. [PubMed: 18701768]
- Ueno E, Tohno E, Soeda S, et al. Dynamic tests in real-time breast echography. *Ultrasound Med Biol*. 1988; 14:53–57. [PubMed: 3055603]
- Varghese T, Bilgen M, Ophir J. Multiresolution Imaging in elastography. *IEEE Trans Ultrason Ferroel Freq Cont*. 1998; 45 (1):65–75.

APPENDIX A

Mini-observer study to select best quality ASSE scan plane per case and preferred display option

We had six imaging planes per case and each plane consisted of multi-compression acquisition of 20 frames. Not all these planes produced unambiguous lesion views on the sonograms and ASSEs. Therefore, one of authors (SC) served as an observer to subjectively select the best image quality ASSE for each case. The ASSE for each plane used in this task was generated based on multi-compression average (MCA) of 20 frames. However, the observer noticed that a few bad quality frames degraded the MCA frame. Instead, it was observed that multi-compression median (MCM) filtered frames do not suffer as much from a few bad frames. An example of such case is shown in figure A.1. Accordingly, three additional observers were asked to rate (blindly) the best image quality between MCA-ASSE and MCM-ASSE for each case (on the already selected best quality plane). Note that these 3 observers did not participate in the main study. Based on this study it was found that 2 out of 3 observers concurred in 5 cases that MCM-ASSE was superior image quality compared to MCA-ASSE. Therefore, the main observer study reported in the paper used MCM-ASSE for these 5 cases.

The Normalized Axial-Shear Strain Area (NASSA) feature

We provide here a brief summary on the NASSA feature used in this study. This feature was described in detail earlier (Thitaikumar et al. 2007), where several candidate features from ASSE were investigated. It was demonstrated that the non-zero axial-shear strain area near the inclusion boundary was an important feature that was extractable even from *in vivo* ASSE. It was shown that by normalizing this area to the size of the inclusion, the inclusion-background modulus contrast, and the applied strain, one could obtain normalized values that directly related to the inclusion bonding condition. It was found that NASSA values were large for firmly-bonded inclusion compared to loosely-bonded inclusions. Therefore, it is reasonable to expect that the NASSA values would cluster towards larger values for cancer cases than for fibroadenomas in the scatter plot shown in figure 4.

ASSE display

Another important issue that was addressed before commencing the main observer study was the desired ASSE display format. Recall that previously ASSE was displayed as stand-alone image with fixed gray scale range, next to the corresponding sonogram (Thitaikumar et al. 2008). However, the display of ASSE as a color-overlay on corresponding sonogram seemed to be advantageous in localizing the axial-shear strain region to relevant lesion of interest. Therefore, two of the observers that participated in the main study performed the following task independently to evaluate the preferred ASSE display. The two observers were presented with a sonogram and a corresponding stand alone grayscale ASSE side by side for each of the 63 cases, one at a time in a random order. The observers then outlined the lesion of interest on the sonogram. Immediately thereafter, a third image widow appeared on the screen that contained color-overlay of segmented ASSE on top of corresponding sonogram. The observers were asked which ASSE display format would be preferred, the response was noted. The analysis of the response showed that in 95% of the cases the two observers preferred the color-overlay of ASSE on corresponding sonogram to the stand-alone grayscale display option.

Details on color-overlay

Only those pixels from ASSE that were deemed to be of good quality (i.e., having corresponding correlation coefficient greater than 0.7) and having axial-shear strain value greater than a contour threshold were overlaid on the corresponding sonogram. The 'jet' color map option was chosen in Matlab[®] to overlay the ASSE. The contour threshold was chosen as 50% of the average-maximum axial-shear strain values near the inclusion boundary. This contour threshold was chosen to be consistent with previously reported feasibility studies on ASSE (Thitaikumar et al. 2007). Clearly, the absolute value of the NASSA depends on the choice of this threshold value. A thorough analysis on the effect of the threshold value on the classification performance is beyond the scope of this work, but is certainly an important aspect that needs to be investigated in future work. This method can be considered a self-normalizing technique where axial-shear strain feature will be normalized for the applied axial strain and inherent elastic modulus contrast simultaneously. Note that if the observer refused to outline a lesion on the sonogram, the average-maximum default value was set to 0.0025 (applied axial compression strain value) for display and segmentation purposes.

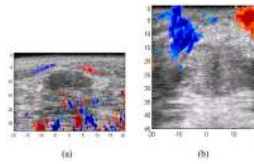


Figure 1.

Examples from the training set showing the axial-shear strain regions of interest as a color-overlay on top of corresponding sonogram of (a) fibroadenoma and (b) cancer. Notice that the axial-shear strain areas (outlined in magenta) due to the cancer were considerably bulkier compared to the slim ones due to the fibroadenoma. The red and the blue colors encode the directional polarity of axial-shear strain (blue-negative, red-positive).

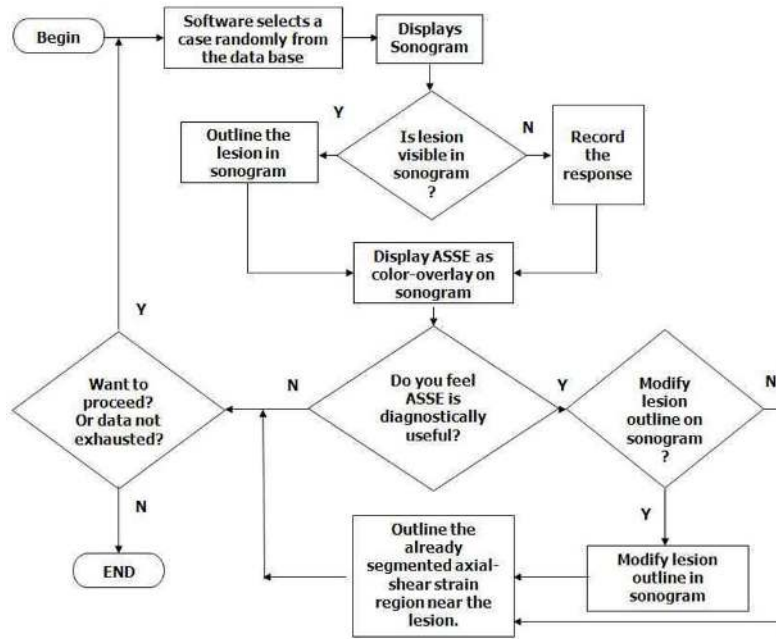


Figure 2. Flowchart describing the step-by-step sequence of how the observer study was performed.

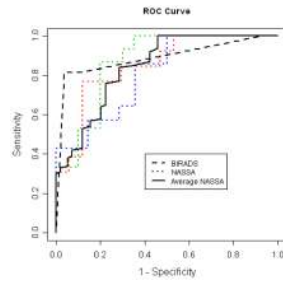


Figure 3.

Plot comparing the ROC curves of the ASSE features value for the three observers (..). The plot also shows the average of the 3 observers ROC curves (solid line) and the ROC curve based on the BIRADS scores (--).

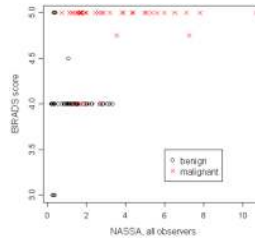


Figure 4. Scatter plot of the NASSA values versus the BIRADS scores. Note that the combination of both axes gives better separation of fibroadenoma (o) and cancer (x) compared to any one axis.

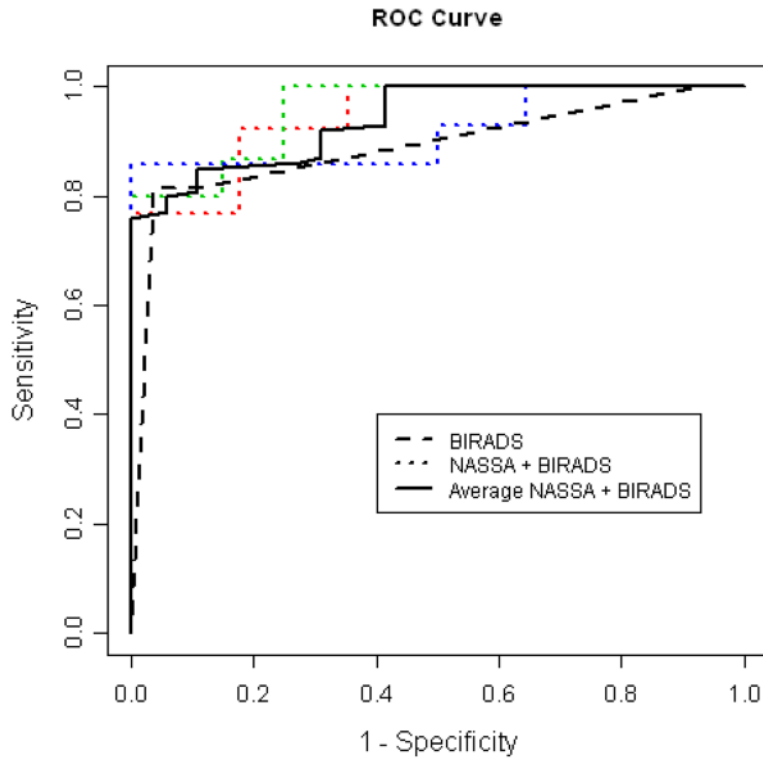


Figure 5. ROC Curves of the logistic regression model scores, using predictors NASSA + BIRADS for the three observers, compared to BIRADS alone.

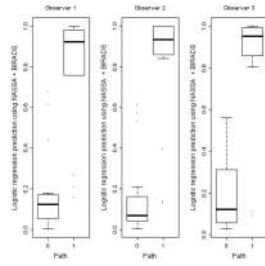


Figure 6.

Boxplots of the predicted values from a logistic regression model using NASSA values and the BIRADS scores as predictors. Path 0 and 1 represents fibroadenoma and cancer, respectively.

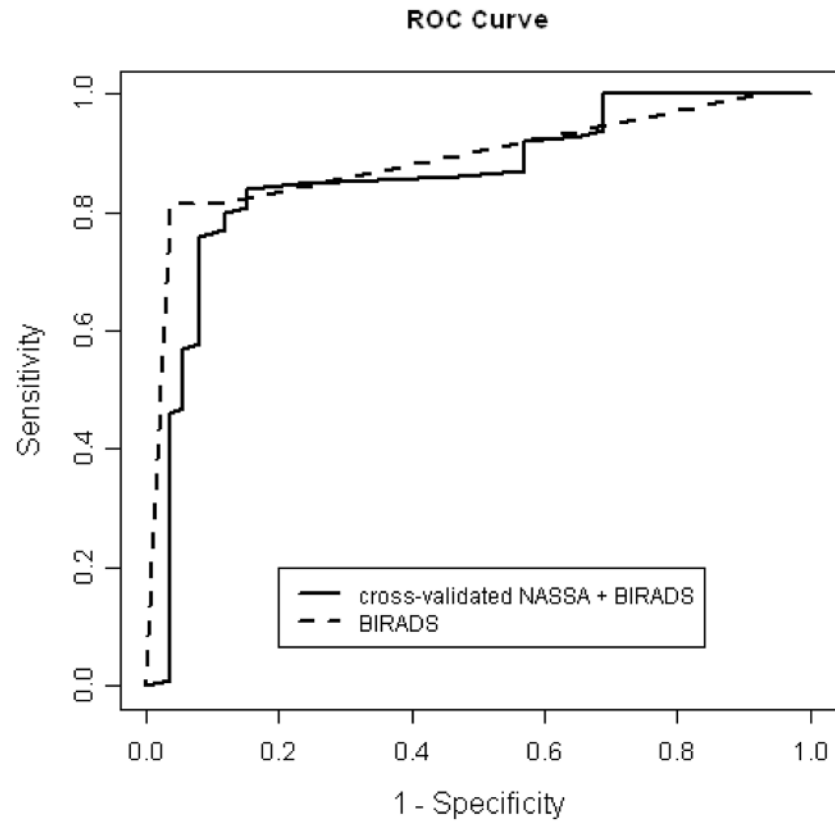


Figure 7. Average ROC Curve of the cross-validated NASSA+BIRADS logistic regression scores compared to ROC curve for BIRADS.

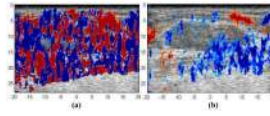


Figure A.1.

An example that demonstrates the improvement in image quality with the use of a MCM-frame filtering (b) as compared to a MCA technique (a).

Table 1
This table presents the summary of the responses from the three observers to the image evaluation task. C-cancer; F-fibroadenoma;

Observer Number	No. of cases with Sonographic ROI (blinded to ASSE)	Additional cases with Sonographic ROI(after looking at ASSE)	No. of cases with Modified Sonographic ROI after looking at ASSE)	% cases where ASSE proved helpful (ratio of the no. of new or modified sonographic cases due to ASSE to total number of cases)	No. of cases with characteristic axial-shear strain pattern in ASSE
1	44 (22C+22 F)	3 (1C+2 F)	2 2(1C+1F)	~11% 5/47	37
2	54 (25C+29 F)	2 (2C)	2 2(2F)	~7% 4/56	42
3	38 (15C+23F)	7 (6C+1F)	2 2(1C+1F)	~20% 9/45	35

Table 2

Logistic Regression analysis of pathology using NASSA and BIRADS as predictors.

	Estimate			Std. Error			Z value		
	obs1	obs2	obs3	obs1	obs2	obs3	obs1	obs2	obs3
Intercept	-17.79	-20.31	-19.02	6.27	6.70	6.83	-2.84	-3.03	-2.79
NASSA	1.14	1.37	1.13	0.69	1.73	0.79	1.65	1.88	1.44
BIRADS	3.62	4.05	3.78	1.37	1.42	1.42	2.64	2.84	2.66